Journal of Pharmaceutical Innovation (2023) 18:874–892
https://doi.org/10.1007/s12247-022-09688-0

ORIGINAL ARTICLE

Design, Development, In Silico, and In Vitro Characterization of Camptothecin-Loaded Mixed Micelles: In Vitro Testing of Verapamil and Ranolazine for Repurposing as Coadjuvant Therapy in Cancer

Kiran S. Patil[1] · Ashok A. Hajare[1] · Arehalli S. Manjappa[2] · Harinath N. More[3] · John I. Disouza[2]

Accepted: 18 September 2022 / Published online: 6 October 2022

Abstract

Purpose Camptothecin has poor solubility, high systemic toxicity, and intrinsic structural instability. To deal with these challenges, present research aimed to develop camptothecin-loaded mixed micelles (CPT MMs) using TPGS and Pluronic® F108 copolymers. Furthermore, our research aimed to test in vitro anticancer activities of non-micellar verapamil and ranolazine for repurposing as coadjuvant therapy with CPT MMs in cancer.

Methods CPT MMs were fabricated by solvent evaporation method and optimized using 3^2 full factorial design. CPT MMs were characterized for % entrapment efficiency (%EE), mean particle size (MPS), zeta potential, surface morphology, % drug loading capacity (%DLC), in vitro drug release, and in vitro cytotoxicity and cell cycle arresting behaviors.

Result The in silico studies revealed decent camptothecin interaction with a cavity of mixed micelles (MMs). CPT MMs composition (H5) is considered optimum based on %EE (94.92 ± 2.46%), MPS (136.9 ± 1.71 nm), zeta potential (−22.9 ± 0.87 mV), and %DLC (1.810 ± 0.02%). TEM image shows self-assembled micelles with spherical shape. CPT MMs showed sustained release profile. The drug-excipient compatibility study revealed no primary incompatibilities. The CPT MMs showed moderately higher IC_{50} values than camptothecin against A549 and B16F10 cells. The non-micellar verapamil and ranolazine when combined with CPT MMs at lower concentrations have resulted in substantially higher cytotoxicity. Whereas, the CPT MMs + ranolazine combination has shown higher cell cycle arresting behavior than CPT MMs + verapamil combination.

Conclusion Elaborative and molecular mechanism–based studies are further needed to validate the repurposing potential of non-micellar verapamil and ranolazine as coadjuvant with CPT MMs in cancer.

Keywords Camptothecin · Verapamil · Ranolazine · Mixed micelles · Cytotoxicity · Cell cycle analysis

✉ Ashok A. Hajare
ashok.hajare@bharatividyapeeth.edu

Kiran S. Patil
kspatil.tkcp@gmail.com

Arehalli S. Manjappa
manjappa.tkcp@gmail.com

Harinath N. More
harinath.more@bharatividyapeeth.edu

John I. Disouza
johnsir4u@gmail.com

[1] Department of Pharmaceutics, Bharati Vidyapeeth College of Pharmacy, Near Chitranagari, Kolhapur 416013, Maharashtra, India

[2] Department of Pharmaceutics, Tatyasaheb Kore College of Pharmacy, Warananagar 416113, Maharashtra, India

[3] Department of Pharmaceutical Chemistry, Bharati Vidyapeeth College of Pharmacy, Near Chitranagari, Kolhapur 416013, Maharashtra, India

Introduction

Cancer kills approximately 70% of people around the globe. It is estimated that 2–3 million new cases are diagnosed each year, and the trend is rising. Lung cancer (LC) has emerged as one of the deadliest diseases that account for the highest number of deaths in 2020 [1]. Non-small cell (NSC) and small cell (SC) carcinoma account for about 85% and 15% of LC, respectively. Ineffective treatment and delay in diagnosis of NSC LC have depicted a low survival rate for 5 years (15%) and poor diagnosis [2]. Chemotherapy is still the most popular cancer treatment, but its low selectivity and serious side effects on normal tissues and multidrug resistance (MDR) have reduced its clinical application [3, 4].

Camptothecin is a monoterpene indole alkaloid commonly identified in *Camptotheca acuminata* and *Nothapodytes nimmoniana* [5]. Camptothecin has been effective

against cancer of the lung, ovarian, breast, stomach, and pancreas [6, 7]. Camptothecin works by binding to type I topoisomerase and the deoxyribonucleic acid (DNA) complex. This produces a ternary complex, which stabilizes it and hinders DNA re-ligation, causing DNA damage and apoptosis [8, 9]. Furthermore, camptothecin has low aqueous solubility, and low stability, at physiological pH; it predominantly exists in a less active carboxylate form [10]. Besides, previously reported literature confirmed that the camptothecin undergoes reversible pH-dependent hydrolysis of the lactone ring and results in toxic carboxylate forms [11]. Even though camptothecin is beneficial in the treatment of a wide range of cancers, drug resistance remains its main problem. Cancer cell resistance and selectivity toward cancer cells are highly complex phenomena. Moreover, the cancer cell resistance mechanisms of camptothecin-based drugs have not been explored extensively [12]. Overexpression of ABCB1 (P-gp/ MDR1) and the resistance produced by P-glycoprotein (P-gp) is pivotal for MDR in cancer [13, 14].

Biocompatible nanocarriers are currently being used to enhance pharmacokinetics and reduce the side effects of cancer treatments [15–17]. Recent developments in the application of nanomaterials have created new frontiers in the treatment of several diseases for the reason that they support sustain drug release, reduce dosing frequency, and increase the residence time of the drugs [18]. For several reasons, mixed micelles (MMs) have been recognized as a promising strategy among the different nano-formulations. It is not only a convenient technique but also it increases the circulatory half-life and accumulation of the drug at the cancer site [19, 20]. Drug-entrapped MMs with a judicious combination of co-polymers is a feasible method to improve the physical, chemical, and biological characteristics of drugs [21–24].

Gao Y. et al. have reported the increased solubility and cytotoxicity of camptothecin for camptothecin-loaded MMs made of Pluronic P105 (P105) and D-α-tocopheryl polyethylene glycol 1000 succinate (TPGS). They also proved increased in vitro cytotoxicity for camptothecin-loaded MMs using a human breast cancer cell line MCF-7 [25]. However, to the best of our knowledge, camptothecin MMs using Pluronic® F108 (PF 108) and TPGS have not been explored yet. The PF 108 is a tri-block copolymer and a terminal primary dihydroxy-functional oligomer. PF108 is an excellent non-ionic surfactant with terminal polar PEG fragments and nonpolar PPG fragments in the center. Its application in drug delivery has resulted in substantially improved mean residential time (MRT) and tumor distribution of drugs, and significant tumor growth suppression without loss of body weight [26–28]. Besides, a longer PEG chain of PF 108 would substantially decrease macrophage uptake and results in the increased circulation time of the drug after the intravenous administration [29]. Moreover, PF 108 is most attractive due to its biocompatibility and low toxicity [24, 30, 31]. TPGS is also a copolymer that is extensively explored for improved delivery of drugs. It's various pharmaceutical and biological applications are reviewed by Kumbhar et al. [32] Therefore, the present study aimed to develop MMs using two chemically distinct copolymers PF 108 and TPGS for camptothecin and tested for their physicochemical properties and in vitro anticancer activities.

Drug repurposing is a strategy wherein the drugs approved for one clinical use are being used for the treatment of another disease [33, 34]. Because the pharmacokinetics, pharmacodynamics, and toxicity profiles of these drugs have already been established in the original preclinical and phase I studies [35, 36], this approach could be cost-effective and offer rapid clinical translation for neoplastic disease treatment [37, 38]. Besides, these non-oncology medications may target both known and unknown cancer vulnerabilities. Moreover, the combined delivery of repurposed therapeutics can reduce the enzymatic metabolism of drugs thereby causing dose reduction and side effects and can also result in synergistic effects thereby achieving better anticancer effectiveness. As antihypertensive drug targets might also influence the development of malignancy, repurposing antihypertensive medications may be relevant as adjuvant therapy in cancer. According to in vitro data for their effectiveness in various cell lines, antihypertensive drugs may have a coadjuvant effect on chemoresistant cell lines, limit cell growth, and boost chemosensitivity in several types of cancer [39–42]. Furthermore, these drugs are also off-patent, orally delivered, and less expensive than alternative cancer therapies [43, 44]. Verapamil (VPM) first-generation P-gp inhibitor is a calcium channel blocker used clinically to treat cardiac arrhythmias [45]. Verapamil can assist in promoting intracellular drug accumulation when used in conjunction with chemotherapeutic drugs [46]. This has been shown in cell lines with leukemia, neuroblastoma, non-small cell lung cancer, and colorectal carcinoma [47–51]. The uses of antihypertensive drugs, including verapamil, as coadjuvant therapy in cancer, are recently reviewed by Carlos-Escalante et al. [44].

The antianginal drug ranolazine (RNZ) has been approved and has a good overall safety record. Voltage-gated Na + channels (VGSCs) are functionally upregulated in cancer, and their activity encourages cellular invasion in vitro and metastasis in vivo [52]. Breast cancer metastasis has been demonstrated to be inhibited in vivo by ranolazine, a therapeutically utilized VGSC inhibitor/anti-anginal drug. Injections of ranolazine greatly decreased the colonization of immune-depressed mice's lungs with human breast cancer cells in vivo, with no noticeable toxic effects. The novel anticancer effects of ranolazine are reviewed by Rouhana et al. [53]. Ranolazine may also lessen the cardiotoxicity of anticancer treatment (trastuzumab, doxorubicin) in mice, opening the door for a clinical trial [54–57]. These novel

anticancer effects of ranolazine may open the way to reposition this "old" drug alone or in combination with other medications.

In the present study (preliminary investigation), the in silico topoisomerase-I inhibition and P-gp inhibition potentials of copolymers (PF108 and TPGS), verapamil, and ranolazine will be determined and compared with camptothecin. Furthermore, the in vitro anticancer activity of non-micellar verapamil and ranolazine alone and in combination with camptothecin MMs (CPT MMs) will be determined using human lung cancer cells (A549) and mouse melanoma cells (B16F10).

Materials and Methods

Materials

Camptothecin was procured from Clearsynth Pvt. Ltd, Mumbai, India. RNZ is supplied by Microlabs Goa. HPLC grade acetonitrile, methanol, and water were purchased from Molychem, Mumbai. VPM, TPGS, PF108, Tween 80, and sucrose were obtained from Sigma Aldrich. Other solvents, chemicals, and reagents used in this study were analytical grade.

Cell Lines and Culture Medium

Mouse B16F10 melanoma and human A549 LC cells were cultured using Dulbecco's Modified Eagle Medium (DMEM) containing 10% of fetal bovine serum (FBS; heat-inactivated), penicillin (100 IU/ mL), and streptomycin (100 µg/mL) in a 5% CO_2 humidified atmosphere at 37 °C. Both B16F10 and A549 cells were dissociated using dissociation solution containing ethylenediamine tetraacetic acid (EDTA; 0.02%), glucose (0.05%), and trypsin (0.2%) in phosphate buffer saline (PBS) [58, 59].

Methods

Investigation of Camptothecin Affinity for MMs Cavity via Molecular Docking Study

ChemDraw® Ultra 8.0 was used to create the circular micelle, which was then exported as a mol file. BIOVIA® Discovery Studio Visualizer was used to convert the micelle mol file to pdb format. Furthermore, pdb file was converted to pdbqt macromolecule by PyRx virtual screening tools per our previous study [24, 60]. Ligand camptothecin was introduced and a universal force field (UFF) was used to minimize energy levels [61]. The designed camptothecin MMs are depicted in Fig. 1C.

Critical Micelle Concentration (CMC)

Gaisford S. et al. reported the Iodine UV spectroscopy method to determine the CMC of micelles [62]. Following the approach outlined by Patil et al., the iodine UV–visible spectrophotometric technique was used to identify the CMC of individual copolymers and their respective mixture [24]. Briefly, a standard solution containing potassium iodide (KI; 2 g) and iodine (I_2; 1 g) in double-distilled water (DDW) was prepared. Accurately, 25 µL of this solution was transferred to different concentrations of aqueous copolymer solutions. These mixtures were stored in the dark for 12 h at room temperature. The absorbance was determined at 366 nm using a UV spectrophotometer [63].

Preparation and Optimization of MMs

The camptothecin loaded with TPGS and PF 108 MMs was fabricated using a solvent evaporation technique. Camptothecin, TPGS, and PF 108 were added to methanol (2 mL) and dissolved using sonication. Drops of this solution were introduced into a beaker containing 10 mL distilled water, which was then stirred at 500 rpm. The stirring proceeded until the entire methanol was evaporated. The resultant camptothecin

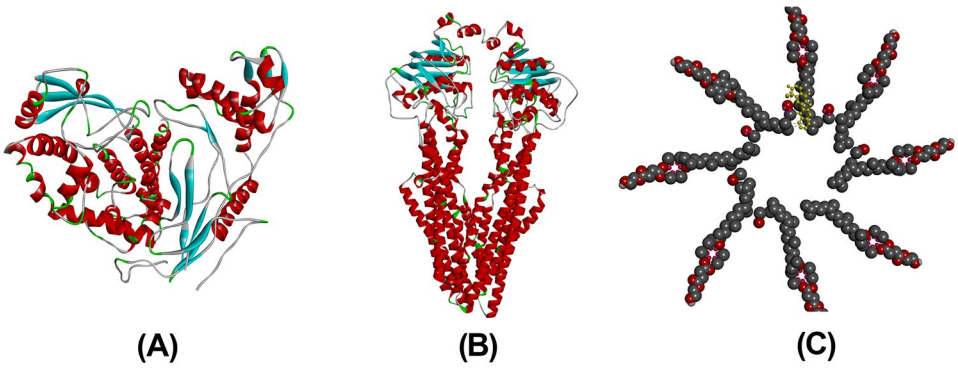

Fig. 1 In silico study: **(A)** 3D structures of human topoisomerase-I; **(B)** 3D structures of P-gp after purification by using BIOVIA Discovery Studio and **(C)** entrapment of camptothecin in MMs

MMs were diluted with 10 mL of distilled water, and the supernatant was collected from the unentrapped camptothecin by centrifugation for 10 min at 5000 rpm [64]. Furthermore, a 3^2 full factorial design was applied to optimize camptothecin MMs, and the influence of independent variables, such as drug-to-polymers ratio (X_1) and concentration of TPGS (X_2), was selected based on risk assessment analysis, whereas %EE (Y_1) and MPS (Y_2) were the dependent variables. Initially, pre-screening was done to estimate independent variables over a wide range. Furthermore, the design space for the individual independent variables was ascertained to achieve a product possessing critical quality attributes (CQAs) within the desired range. The levels of each factor were set to − 1, 0, and + 1 to optimize the material attributes used in the experimental work. Drug to polymer molar ratio (X_1) was taken with coded values − 1 (1:6), 0 (1:7), and + 1 (1:8); likewise, the TPGS concentration (X_2) was taken with coded values − 1 (8.1 mg), 0 (12.2 mg), and + 1 (16.3 mg) respectively. The design matrix for all formulations is presented in Table 2. The data obtained for nine compositions were statistically analyzed using Design Expert® VR software [24, 64]. Contour plots were generated to examine the impact of variables on the responses. Statistical significance is designated by the *p*-values ($p < 0.05$). The coefficient of magnitude was calculated using polynomial equations.

Characterization of Camptothecin MMs

% Entrapment Efficiency (%EE) and %Drug Loading Capacity (%DLC)

Accurately, 0.1 mL of camptothecin MMs was diluted to 5 mL with methanol and bath sonicated for 2 min. Camptothecin content was determined spectrophotometrically at 219 nm. The following equations were used to estimate %EE and %DLC of camptothecin MMs [65].

$$\%EE = \frac{\text{Weight of camptothecin in camptothecin MMs}}{\text{Weight of camptothecin taken initially}} \times 100$$

$$\%DLC = \frac{\text{Weight of camptothecin in camptothecin micelles}}{\text{Weight of camptothecin taken initially} + \text{Weight of (PF108 and TPGS)}} \times 100$$

Mean Particle Size and Zeta Potential

MPS and zeta potential of camptothecin MMs were detected by Horiba® SZ-100 particle size analyzer. It detects the MPS and zeta potential by employing dynamic light scattering and laser doppler anemometry. All of the results were recorded in triplicate at 25 ± 5 °C and mean standards were determined [63].

Transmission Electron Microscopy (TEM)

The camptothecin MM (H5) composition was visualized using TEM. Concisely, a drop of formulation H5 was placed on a copper grid and entirely air-dried. Furthermore, one drop of phosphotungstic acid solution (2%) was placed on a smear of micelles prepared on the grid, air-dried, and analyzed using TEM (Jeol Model JM 2100) [66].

Drug-Excipient Compatibility Study

Lyophilization of Camptothecin MMs

Accurately measured 1 mL of camptothecin MMs (H5) optimized batch composition and 20% w/v sucrose was filled in glass vials (3 mL capacity). The rubber closures were positioned as half-closed. The solutions were frozen at − 20 °C for 12 h in the deep freezer. The pre-frozen vials were lyophilized in Martin Christ lyophilizer at a shelf temperature of − 42 °C while condenser temperature was maintained at − 50 °C, and 0.1 mBar vacuum was applied for 48 h as per previous literature [67, 68]. The dried formulation was further subjected to secondary drying by keeping vials in the vacuum chamber (pressure 0.06 mBar) for 12 h and sealed under vacuum. Camptothecin MM lyophilized formulations were stored at 2–8 °C and used for further characterization.

Fourier Transform Infrared Spectroscopy (FTIR)

FTIR spectra of camptothecin, TPGS, PF108, and camptothecin MM compositions were recorded over the wavelength range from 400 to 4000 cm^{-1} using FTIR spectrophotometer (Agilent, Alpha 100,508) to investigate camptothecin compatibility with TPGS and PF108 [24].

Differential Scanning Calorimetry (DSC)

The thermal characteristics and interaction between the camptothecin, TPGS, and PF108 were investigated utilizing (DSC; SDT Q600 V20.9 Build 20) of plain camptothecin and optimized camptothecin MMs. Camptothecin and

camptothecin MMs samples (5–10 mg) were subjected to heating starting from 0 to 500 °C with a scanning rate of 10 °C/min in a dry nitrogen atmosphere and thermograms were obtained. An empty aluminum pan served as the reference material [69].

Powder X-ray Diffraction Analysis

Powder X-ray diffraction (PXRD) investigation was done to validate potential drug interactions with excipients used. The XRD pattern of plain camptothecin and optimized camptothecin MMs was analyzed by X-ray diffractometer (D8 Advance, Bruker, Germany) with a Cu, Kα radiations stable at 40 kV and 100 mA at ($\lambda = 1.54$ Å) with increments of 0.02° from 5 to 60° diffraction angle (2θ) at 1 s/step [69].

In Vitro Drug Release Study

The dialysis tube technique was used to compare in vitro release patterns of plain camptothecin dispersion (2.5 mg drug was dispersed in distilled water and transferred to dialysis tube) and camptothecin MMs (equivalent to 2.5 mg). These dispersions were introduced separately into dialysis tubes (Himedia, 12,000 Dalton molecular weight cutoff) and sealed. The tubes were placed into beakers containing 50 mL of PBS of pH 7.4. Tween 80 (equivalent to 0.5% v/v) was added to PBS to retain sink condition. Throughout the study, the temperature of the dissolution medium was maintained at 37 ± 2 °C with continuous stirring at 150 rpm. Cumulative drug release was performed over 72 h at time intervals 2, 4, 6, 8, 24, 36, 48, 60, and 72 h. The 1 mL of release medium was withdrawn each time and replaced with equal volumes of plain PBS containing 0.5% v/v Tween 80. The sample supernatant was spectrophotometrically analyzed for camptothecin content at 225 nm [64, 70].

Investigation of P-gp and Topoisomerase-I Inhibitory Potential Using Molecular Docking

The Vina Wizard Tool in PyRx 0.8 was used to execute the molecular docking study [45]. Camptothecin, verapamil, TPGS, and PF-108 structures (sdf file) were obtained from the PubChem National Library of Medicine. The energy was minimized by the universal force field (UFF) [60, 61]. Human topoisomerase-I and p-glycoprotein structures were taken from the RCSB Protein Data Bank (PDB) as entries 1R49 and 7A6E, respectively Fig. 1A and B. P-gp ABCB1 was chosen for the docking study as ABCB1 is an ATP-binding cassette transporter, related to cancer cell MDR. Enzyme structures were optimized and purified for docking. In order to simulate molecular docking, the 3D grid box for human topoisomerase-I (size_x = 67.8377 Å; size_y = 71.4027 Å; size_z = 70.0305 Å) and P-gp (size_x = 65.1718 Å; size_y = 117.5754 Å; size_z = 66.4700 Å) was designed using Autodock tool. BIOVIA Discovery Studio Visualizer was employed to identify and note the protein's active amino acid residues. In silico study was performed in line with the previously outlined procedure by Khan et al. [24, 71, 72].

In Vitro Cytotoxicity

In vitro cytotoxicity of different test samples (camptothecin, verapamil, ranolazine, camptothecin MMs, combinations of camptothecin plus non-micellar verapamil and ranolazine, and combinations of camptothecin MMs plus non-micellar verapamil and ranolazine) was screened using MTT dye reduction assay against mouse B16F10 melanoma and human A549 lung cancer cells. Initially, the camptothecin, verapamil (VPM), ranolazine, and CPT MMs were tested at concentration range (0.001 to 100 µM); furthermore, there combined effects of camptothecin + verapamil or ranolazine and combinations of camptothecin MMs + verapamil or ranolazine were tested in the concentration range (0.0001 to 100 nM). The study was performed as per the previous report [24]. Briefly, 50,000 cells were added to each well of the 96-well microtiter plate using 100 µL of cell suspension. Following a 24 h incubation period, the supernatant from each well was replaced with 100 µL of varying concentrations of the above test substances. The plain drugs were dissolved in dimethyl sulfoxide (DMSO) while the camptothecin MMs formulation was dissolved in the medium to carry out the anticancer activity. The plates were then incubated at 37 °C for 48 h in a 5% CO_2 atmosphere. After incubation, the test solutions in the wells were replaced with 100 µL of MTT solution (0.05 mg), and plates were incubated at 37 °C in a 5% CO_2 atmosphere for 4 h. MTT solution was replaced with DMSO (100 µL) and plates were gently shaken to solubilize the formed formazan crystals. The absorbance was then measured using a microplate reader at a wavelength of 590 nm. The % growth inhibition was calculated, and the concentration of test drug needed to inhibit 50% cell growth (IC_{50}) was generated from the dose–response curves for each cell line [73].

Cell Cycle Analysis

1×10^6 cells were seeded and cultured in a 6-well plate containing 2 mL of serum-free medium for 24 h. Cells were then incubated with 2 mL of different test solutions of camptothecin (CPT), camptothecin (CPT MMs), verapamil (VPM), and ranolazine (RNZ), CPT MMs plus VPM mixture, and CPT MMs plus RNZ mixture for another 48 h. The test solutions were screened at two different concentrations (0.5 and 1 µM). Cells were harvested and then centrifuged at 2000 rpm for 5 min at room temperature to

obtain the cell pellet. Post-washing (in 2 mL of 1 × PBS), the cells were fixed in sheath fluid (300 µL) followed by drop-by-drop addition of chilled 70% ethanol (1 mL). This mixture was gently shaken and another 1 mL of chilled 70% ethanol was added at once. The cells were then stored overnight at 4 °C. Post fixing, the cells were centrifuged (at 2000 rpm for 5 min); the obtained cell pellet was washed (twice with 2 mL of cold 1 × PBS) and dispersed in 450 µL of sheath fluid containing propidium iodide (0.05 mg/mL) and RNaseA (0.05 mg/mL). The above mixture was then incubated in the dark for 15 min. The percentage of cells in various stages of the cell cycle in treated and untreated populations was determined using FACS Caliber (BD Biosciences, San Jose, CA). A minimum of 10,000 cells was acquired for each sample [74, 75].

Statistical Analysis

Formulation and optimization data are averages of triplicates and expressed as means with ± SDs. The influence of various variables of development of formulation on the response variables was statistically evaluated by applying ANOVA at 0.05 levels using the Design-Expert® version (Stat-Ease Inc.). The polynomial equation, 3D response surface graphs, and contour plots to study the interaction of independent variables on dependent variables were established by applying ANOVA using Design-Expert® software. Further data are presented as the mean ± standard deviation of three independent experiments. GraphPad Prism software version 8 (GraphPad Software, Inc., La Jolla, CA, USA) was used for statistical analysis. The obtained results were analyzed using one-way ANOVA and two-way ANOVA, and $p < 0.05$ was considered to indicate a statistically significant difference.

Results and Discussion

TPGS is a good solubilizer. An amphiphilic nature of TPGS shows a hydrophilic polar head and a lipophilic alkyl tail. Additionally, previously reported studies reveal that TPGS strongly enhances the cytotoxicity of various cancer drugs in a highly efficient manner [76]. It has also been reported that TPGS micellar stability decreases upon intravenous administration, resulting in easy dissolution by plasma. To overcome these issues, TPGS is used in combination with PF108 to form camptothecin MMs [76, 77]. PF108 is a tri-block (PEG-PPG-PEG) copolymer that has excellent surfactant properties. It has been extensively employed in tumor distribution and tumor growth suppression applications in various nanoformulations [27, 78].

In Silico Analysis of Camptothecin and MMs Interaction

Camptothecin showed excellent binding affinity toward the polar head of the MMs cavity with − 4.5 kcal/mol binding energy. It made a hydrogen bond with the polar head of MMs and 4 hydrophobic bonds with the non-polar tail, Fig. 1C. Most interestingly, camptothecin seems to form a hydrogen bond with the oxygen atom of PF108 with a bond length of 2.96105 Å, predicting its significant role in drug entrapment. Owing to π-orbitals of the aromatic ring system, camptothecin has hydrophobic interactions through C-26, C-34, C-35, and C-22 of TPGS with bond lengths of 4.30924 Å, 5.28364 Å, 5.04764 Å, and 4.35697 Å, respectively. All these interactions confirm the camptothecin entrapment into the polar head of the micelle, the rationale behind the formulation of the micellar drug delivery system. The ligand energy, binding affinity, and rmsd values are represented in Table 1.

CMC of Polymers and MMs

CMC is the least concentration of the amphiphilic molecules required to self-assemble into micelles in a solution. The CMC of copolymers can be determined using a variety of techniques including iodine UV spectroscopy and pyrene fluorescence spectroscopy. Ronak et al. compared iodine UV–visible spectrophotometric method and pyrene fluorescence spectroscopy for determining the CMC of Solutol HS-15 polymeric micelles and their MMs with phospholipon 90H. Furthermore, he revealed almost the same CMC value for both methods [79]. In the present study, the iodine UV–visible spectrophotometric method was used to determine the CMC of polymers and mixed polymers. In this method, iodine was used as a hydrophobic probe with various copolymer concentrations. Solubilized I_2 prefers to interact in the hydrophobic microenvironment of micelles to maintain the saturated aqueous concentration of I_2 resulting in the conversion of I_3 to I_2 from excess KI in the solution [73, 75]. Plain TPGS, PF 108, and camptothecin MMs had CMC values of 0.01 mM, 0.033 mM, and 0.023 mM, respectively. Camptothecin MMs with a lower CMC value suggest micellization and micellar stability. These findings were consistent with the previous studies [24, 28].

Preparation and Optimization of Camptothecin MMs

Out of nine camptothecin MMs formulations, composition H5 was predicted as optimized based on %EE (94.92 ± 2.46%), MPS (136.9 ± 1.71 nm), PDI (0.326 ± 0.7), zeta potential (− 22.9 ± 0.87 mV), and %DLC (1.810 ± 0.02%). Due to the presence of ionisable-hydroxyl (-OH) functional groups in TPGS and PF108,

Table 1 binding affinities, ligand energy, RMSD ub/lb values of molecules, with MMs cavity, topoisomerase-I, and P-gp

Ligand name	Ligand energy (kcal/mol)	Conformers	Binding affinity (kcal/mol)	rmsd/ub	rmsd/lb
Camptothecin with MMs (TPGS and PF108) cavity					
Camptothecin	418.60	1	−4.5	0	0
		2	−3.9	27.819	25.975
		3	−3.9	9.753	5.87
		4	−3.9	29.089	25.168
		5	−3.9	7.857	4.123
		6	−3.8	29.023	24.703
		7	−3.8	9.264	5.361
		8	−3.7	18.717	14.337
		9	−3.6	30.973	27.979
Molecules with topoisomerase-I (PDB ID: 1R49)					
Camptothecin	418.60	1	−7.9	0	0
		2	−7.9	7.367	3.507
		3	−7.5	3.249	2.017
		4	−7.5	31.303	30.486
		5	−7.4	27.808	24.032
		6	−7.3	39.167	36.299
		7	−7.3	24.919	20.618
		8	−7.2	3.575	1.568
		9	−6.9	22.27	20.99
PF-108	1428.06	1	−3	0	0
		2	−2.7	38.261	38.041
		3	−2.6	33.129	32.618
		4	−2.5	22.22	22.011
		5	−2.5	34.627	34.411
		6	−2.5	32.785	32.653
		7	−2.4	28.403	27.678
		8	−2.3	30.002	29.494
		9	−2.3	30.783	30.533
TPGS	910.18	1	−6.6	0	0
		2	−6.3	34.163	31.335
		3	−6.2	3.292	2.03
		4	−6.1	2.367	1.666
		5	−6.1	2.966	2.104
		6	−6.1	32.534	29.253
		7	−6	32.979	29.309
		8	−5.9	31.579	28.64
		9	−5.9	11.711	4.483
Ranolazine	405.57	1	−7.2	0	0
		2	−7	10.895	4.102
		3	−6.9	2.418	1.171
		4	−6.9	31.822	29.55
		5	−6.7	31.027	28.169
		6	−6.6	31.519	28.332
		7	−6.5	10.793	4.636
		8	−6.4	10.426	2.473
		9	−6.3	28.126	25.084

Table 1 (continued)

Ligand name	Ligand energy (kcal/mol)	Conformers	Binding affinity (kcal/mol)	rmsd/ub	rmsd/lb
Verapamil	865.17	1	−5.8	0	0
		2	−5.6	34.149	31.746
		3	−5.6	36.354	33.96
		4	−5.6	33.4	29.578
		5	−5.6	25.101	21.63
		6	−5.5	7.16	3.786
		7	−5.4	34.036	32.356
		8	−5.4	36.019	33.69
		9	−5.3	33.445	30.722
with P-gp (PDB ID: 7A6E)					
Ranolazine	405.57	1	−8	0	0
		2	−8	8.356	3.108
		3	−8	15.69	11.315
		4	−8	9.362	3.22
		5	−7.9	3.194	1.844
		6	−7.6	8.38	2.544
		7	−7.6	16.825	12.569
		8	−7.5	4.731	2.951
		9	−7.3	5.158	2.549

camptothecin MMs have a negative zeta potential value. These groups dissociate, leaving a negative charge and releasing H + ions into the water around them [24]. Moreover, as per the previous literature, the negative zeta potential of MMs could be correlated to the presence of TPGS [80]. The MPS and zeta potential of the H5 composition are shown in Fig. 2A and B, respectively. A brief overview of the compositions obtained using Design Expert along with their characterization is presented in Table 2.

Optimization of Formulation

The formulation was optimized by using 3^2 full factorial design. The formulation was optimized using a statistical approach to study the effect of all the factors and their interaction on responses. The design is useful to investigate the quadric effects. Hence, the design was employed for the development of a statistically optimized formulation with minimum experimental runs. The detailed optimization of formulation and effect of an independent variable

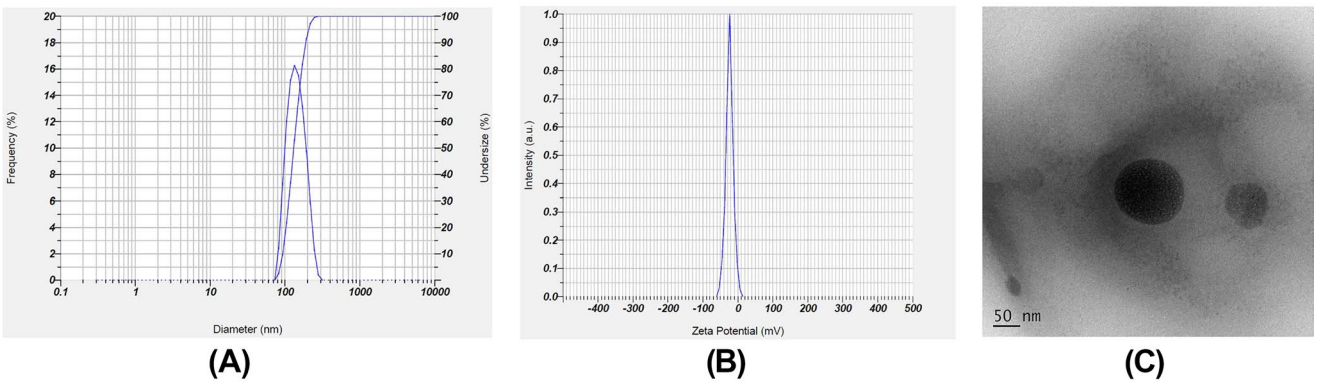

Fig. 2 **(A)** MPS, **(B)** zeta potential, and **(C)** TEM image of optimized composition of camptothecin MMs (H5)

Table 2 Camptothecin MMs compositions identified using 3^2 full factorial design and their responses

Formulation Code	Drug (mg)	Drug:polymer molar ratio	TPGS: PF108 (molar ratio)	TPGS (mg)	PF 108 (mg)	%EE (%)	Mean particle size (nm)	Polydispersity index (PDI)	Zeta potential (mV)
H1	2.5	1:6	2:4	8.1	414	88.08 ± 2.35	186.50 ± 1.26	(0.540 ± 0.063)	− 21.00 ± 1.03
H2	2.5	1:6	3:3	12.2	310	87.40 ± 2.74	153.20 ± 2.13	(0.310 ± 0.027)	− 21.36 ± 0.74
H3	2.5	1:6	4:2	16.3	207	86.02 ± 2.67	142.50 ± 1.37	(0.404 ± 0.056)	− 21.64 ± 0.29
H4	2.5	1:7	2:5	8.1	518	95.12 ± 1.35	201.20 ± 2.37	(0.312 ± 0.056)	− 21.70 ± 1.26
H5	2.5	1:7	3:4	12.2	414	94.92 ± 2.46	136.90 ± 1.71	(0.326 ± 0.072)	− 22.90 ± 0.87
H6	2.5	1:7	4:3	16.3	310	93.68 ± 3.22	137.52 ± 0.78	(0.422 ± 0.012)	− 22.87 ± 1.16
H7	2.5	1:8	2:6	8.1	621	96.06 ± 2.35	296.70 ± 2.13	(0.284 ± 0.049)	− 22.17 ± 0.95
H8	2.5	1:8	3:5	12.2	518	93.34 ± 1.28	273.00 ± 1.86	(0.461 ± 0.029)	− 22.35 ± 0.62
H9	2.5	1:8	4:4	16.3	414	91.76 ± 3.16	263.20 ± 1.89	(0.285 ± 0.035)	− 21.90 ± 0.78

on responses has been studied using Design expert® and evaluated using ANOVA.

Formulation Variable: Particle Size

The effect of independent variables on particle size is described by the quadratic Eq. (1).

$$Y_1 = +146.99 + 58.45A - 23.53B + 2.62AB + 60.81A^2 + 17.07B^2 \quad (1)$$

where Y_1 is the particle size, A is the drug:polymer molar ratio, and B is the amount of TPGS. This equation shows that both independent variables have a noticeable influence on the micelle size. The smallest MPS is required to enhance the rate and extent of cellular uptake that can achieve improved systemic circulation and therapeutic efficacy of camptothecin. The mean size of micelle increases with increasing the concentration of drug:polymer from 1:6 to 1:8. Furthermore, an increase in TPGS amount resulted in a decrease in MPS of composition H1 to H5. The formulation H5 has shown the smallest MPS (136.9 ± 1.71 nm) of all other compositions. The model's F-value of 40.96 indicates that it is significant ($p < 0.05$). In this case, A, B, and A^2 are significant model terms ($p < 0.05$).

The predicted R^2 value of 0.8612 is in good agreement with the adjusted R^2 of 0.9615, signifying a good fit. The adequate precision ratio of 15.02 and standard error 5.09 specifies an adequate signal. Hence, the quadratic model was employed to explore design space. The 3D-response surface plots, Fig. 3A, revealed the impact of independent variables on micelle size. The micelle particle size reduced significantly as the concentration of A and B increased.

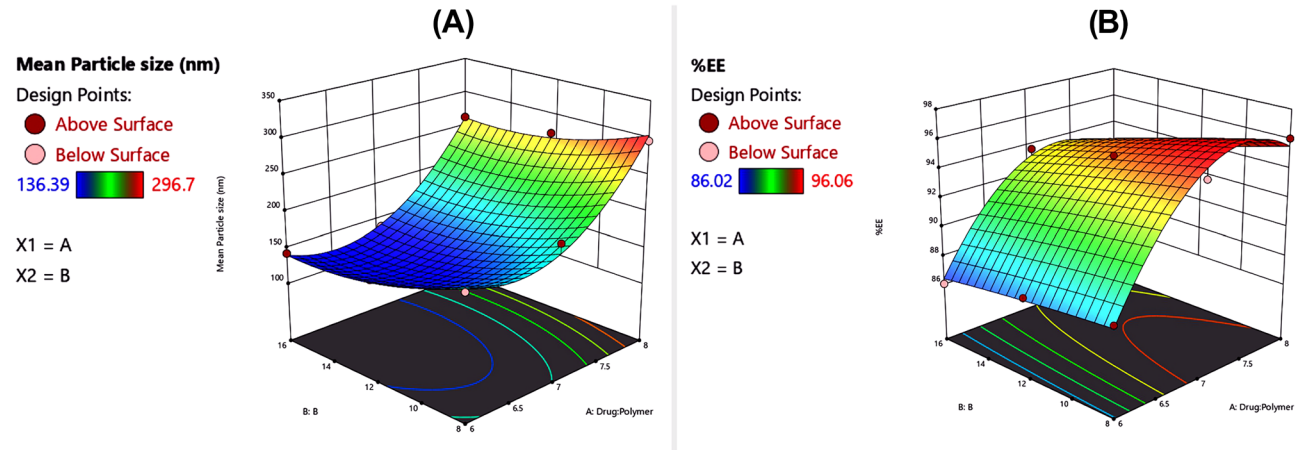

Fig. 3 3-D surface plots **(A)** MPS and **(B)** EE%

Formulation Variable: % EE

The % EE of the camptothecin compositions is listed in Table 2. The composition H5 shows the highest %EE (94.92 ± 2.46%), while the H7 composition shows the lowest (86.02 ± 2.67%). The following polynomial quadratic equation can explain the impact of independent variables on the % EE.

$$Y_2 = 94.64 + 3.28\ A - 1.3B - 0.56AB - 4.13A^2 - 0.1B^2 \quad (2)$$

where Y_2 is the %EE, A is the amount of drug:polymer molar ratio, and B is the amount of TPGS. According to Eq. (2), it is shown that amount of drug:polymer has a favorable effect on the drug entrapment at1:6 and 1:7 ratios, whereas at 1:8 ratio, it shows a negative effect. The high coefficient value of A relates to the amount of drug:polymer which had a significant effect on the %EE of camptothecin compared to the TPGS alone.

The F-value 44.95 infers that the model is significant ($p < 0.05$). There is only a 0.51% probability that a model F-value this large could arise due to noise. B and A^2 are significant model terms ($p < 0.05$). The predicted R^2 value of 0.8469 is in considerable agreement with the adjusted R^2 of 0.9649. The acquired ratio of 16.54 and standard error 0.52 specifies an adequate signal. Therefore, the quadratic model can be employed to explore the design space. The 3D-surface plots in Fig. 3B showed that %EE increases with an increase in the amount of TPGS. On the contrary, the %EE of camptothecin initially increased with a rise in the amount of drug:polymer concentration from 1:6 to 1:8 ratio.

Characterization of Optimized Camptothecin MMs

TEM Analysis

The morphology of optimized camptothecin MMs was evaluated through photographic elucidation by TEM. The self-assembled camptothecin MMs, Fig. 2C, are well dispersed as individual particles with spherical shapes.

Drug-Excipient Compatibility Study

FTIR Spectroscopy

The overlain of the FTIR spectrum of camptothecin (plain), PF108, TPGS, and optimized formulation (H5) is presented in Fig. 4A. FTIR spectrum of plain camptothecin showed – OH stretching at 3558.56 cm^{-1}, stretching of C–C(= O)-O for cyclic ester (lactone) at 1718.48 cm^{-1}, pyridone, C = C, and CN stretching observed at 1564 cm^{-1}, and1447 cm^{-1} and pyridone C–C(= O)-O stretching at 1649.92 cm^{-1}. The FTIR spectra of optimized formulation (H5) retained all of the characteristic absorption bands of camptothecin. These findings signify an absence of interaction between camptothecin, TPGS, and PF108 in the camptothecin MMs.

DSC Analysis

The melting temperatures in the DSC spectra, Fig. 4B, are sharply exothermic at 278.326 °C and endothermic at 346.91 °C confirming the camptothecin [2, 3, 49, 50]. DSC thermograms of the camptothecin MMs composition specify

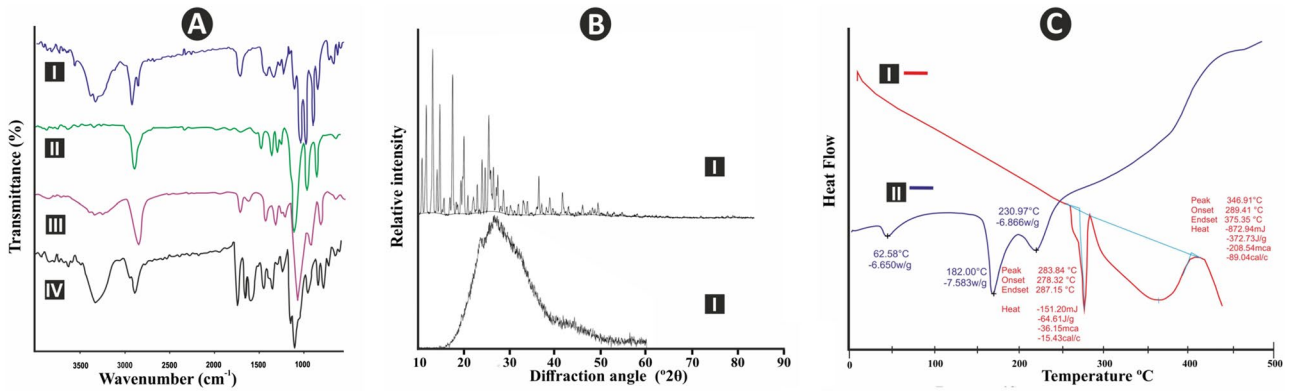

Fig. 4 Drug-excipient interaction studies: **(A)** Overlain FTIR spectra (I) camptothecin, (II) PF108 (III) TPGS, and (IV) optimized formulation; **(B)** overlain DSC thermograms (I) camptothecin, (II) lyophilized optimized (H5) formulation and; **(C)** overlain P-XRD (I) camptothecin (plain) and (II) lyophilized optimized formulation (H5)

the integrity of the drug. Camptothecin melting point peak in its MMs disappeared, representing its crystalline form conversion to the amorphous form, indicating the possibility of molecular dispersion in a matrix material [24].

P-XRD Analysis

The P-XRD patterns of camptothecin and camptothecin MMs (H5) formulation are illustrated in Fig. 4. PXRD of camptothecin (plain) displayed typical strong diffraction peaks with high energy, signifying its crystallinity. Standard diffraction peaks indicating crystallinity of camptothecin were observed at the 2θ diffraction angles of 9.0°, 11.9°, 13.3°, 17.7°, 20.2°, 24.9°, 25.4°, and multiple peaks within 30 − 50°. However, in the case of optimized camptothecin MMs, these peaks were significantly broadened with a decrease in peak intensities, revealing partial amorphization [81].

In Vitro Drug Release Study

In PBS (pH 7.4) containing 0.5% w/v Tween 80, plain camptothecin release from dispersion (2.5 mg drug was dispersed in distilled water and transferred to dialysis tube) was more than 90% of the camptothecin within 4 h. Tween 80 aids in the conservation of the sink condition. Conversely, drug release from camptothecin MMs (78.65 ± 2.12% w/v; 72 h) was considerably sustained ($p < 0.01$). Lan Zhang et al. reported the sustained release of self-assembled docetaxel-loaded polymeric micelles over the 96 h [82]. However, Dabholkar et al. reported very slow (NMT 20% after 48 h) in vitro release of paclitaxel from MMs in PBS pH 7.4 under sink conditions [83]. Camptothecin sustained release by camptothecin MMs precludes early premature drug release and thus lower exposure to blood components and other normal tissues [24, 63]. Besides, this feature of MMs may result in its increased accumulation in tumors and improve the therapeutic efficacy of camptothecin [84].

Molecular Docking

Investigation of P-gp and Topoisomerase-I Inhibitory Potential

The drug efflux mechanism of MDR in tumor cells is predominantly arising because of overexpression of P-gp. A molecular docking study discloses the significant inhibitory potential of verapamil, TPGS, and PF 108, against P-gp. Hence, in silico molecular docking study affirms that camptothecin MMs can efficiently inhibit MDR-associated cancer, thereby backing the study rationale.

The study was further extended to investigate the inhibitory potential of camptothecin, PF108, TPGS, ranolazine, and verapamil on topoisomerase-I. The binding affinities and ligand energies of the enzymes are presented in Table 2. In silico study factors such as active amino acid residues responsible for the interaction, bond length, and types of bonds are presented in Table 3. Camptothecin exhibited − 7.9 kcal/mol binding affinity with an allosteric site of topoisomerase-I forming two conventional hydrogen bonds. TPGS (− 6.6), ranolazine (− 7.2), and verapamil (− 5.8) also show significant binding affinity with topoisomerase-I. The docking poses (3D and 2D) of the molecules (camptothecin, PF108, TPGS, ranolazine, and verapamil) with the topoisomerase I and verapamil with P-gp are presented in Fig. 5. These results of molecular docking are consistent with the previously reported work and could be beneficial for clinical studies [24].

B16F10 and A549 Cell Growth Inhibition Study

All tested samples exhibited concentration-dependent cytotoxicity against both B16F10 and A549 cells (Fig. 6). The IC_{50} values of all tested samples are presented in Table 4. The plain camptothecin and camptothecin MMs showed almost similar cytotoxicity against both B16F10 and A549 cells. Whereas, verapamil and ranolazine not showed significant cytotoxicity against both the cells. In the present study, the influence of lower concentrations of verapamil and ranolazine on the in vitro cytotoxic nature of lower concentrations of plain camptothecin and its MMs were tested. The results revealed a substantially higher cytotoxic nature (lowest IC_{50} values) of tested combinations at lower concentrations. The MMs, alone and in combination, showed moderately lower cytotoxicity when compared to other test samples. This could be correlated to sustained release of camptothecin from MMs and stearic hindrance caused by hydrophilic long PEG chain of PF 108 that further results in delayed cell uptake [24, 29, 85]. The verapamil, alone and in combination, caused somewhat higher cytotoxicity than ranolazine. Besides, the B16F10 cells are found moderately more sensitive to all tested formulations than A549 cells.

The current study revealed the superior in vitro cytotoxicity of camptothecin and its MMs when combined with verapamil and ranolazine at a very low dose than higher concentrations of individual test substances. Thus, by using these combinations at lower doses, few chemotherapy hurdles such as the dose-dependent toxicity, cost of chemotherapy, and primary indications of repurposed drugs could be minimized. However, further in vivo studies are needed to ascertain these facts.

As the novel anticancer applications of verapamil and ranolazine (as described in the introduction) have already been explored, the present study is undertaken to test the possibilities of using them as coadjuvants with

Table 3 Types of bond and the bond length, of the active amino acid residues involved in the interaction

Active amino acid residues	Bond length (Å)	Bond type	Bond category
with topoisomerase-I (PDB ID: 1R49)			
Camptothecin			
A:ARG364	2.58553	Hydrogen bond	Conventional hydrogen bond
A:HIS367	2.08485	Hydrogen bond	Conventional hydrogen bond
A:LYS493	4.3	Electrostatic	π-cation
A:ARG532	4.42138	Hydrophobic	π-alkyl
A:ARG488	5.05686	Hydrophobic	π-alkyl
A:ARG532	4.50476	Hydrophobic	π-alkyl
PF-108			
HIS222	2.46685	Hydrogen bond	Conventional hydrogen bond
TYR338	3.70837	Hydrogen bond	Carbon hydrogen bond
PRO225	4.7406	Hydrophobic	Alkyl
ILE350	4.63493	Hydrophobic	Alkyl
ILE427	4.0951	Hydrophobic	Alkyl
TPGS			
A:ARG488	1.92261	Hydrogen bond	Conventional hydrogen bond
A:GLY490	1.9417	Hydrogen bond	Conventional hydrogen bond
A:ARG590	2.17283	Hydrogen bond	Conventional hydrogen bond
A:ARG488	3.54887	Hydrogen bond	Carbon hydrogen bond
A:LYS493	3.73441	Hydrogen bond	Carbon hydrogen bond
A:ARG590	3.54719	Hydrogen bond	Carbon hydrogen bond
A:LYS493	4.80912	Electrostatic	π-cation
A:ARG532	4.34473	Hydrophobic	Alkyl
A:ARG532	5.15397	Hydrophobic	Alkyl
A:ARG488	3.7289	Hydrophobic	Alkyl
A:ARG364	3.92851	Hydrophobic	Alkyl
A:ARG532	4.70179	Hydrophobic	Alkyl
A:ARG532	4.18986	Hydrophobic	π-alkyl
A:PHE361	5.05759	Hydrophobic	π-alkyl
A:HIS367	5.1663	Hydrophobic	π-alkyl
Ranolazine			
LYS587	3.62971	Hydrophobic	π-sigma
ARG532	4.35236	Hydrophobic	Alkyl
ALA499	3.89695	Hydrophobic	Alkyl
ARG532	5.14151	Hydrophobic	Alkyl
ARG488	4.94833	Hydrophobic	π-alkyl
ARG364	4.94922	Hydrophobic	π-alkyl
Verapamil			
ARG532	2.08748	Hydrogen bond	Conventional hydrogen bond
ASP533	2.60989	Hydrogen bond	Conventional hydrogen bond
LYS493	4.40848	Electrostatic	π-cation
ALA499	3.67347	Hydrophobic	Alkyl
ARG364	4.55572	Hydrophobic	Alkyl
ARG532	4.48682	Hydrophobic	π-alkyl
with P-gp (PDB ID: 7A6E)			
Ranolazine			
GLN838	2.17014	Hydrogen bond	Conventional hydrogen bond
PHE994	3.7065	Hydrophobic	π-sigma
PHE239	3.80878	Hydrophobic	π-π stacked
VAL991	4.21092	Hydrophobic	Alkyl
ILE299	4.08689	Hydrophobic	Alkyl
ALA834	5.05274	Hydrophobic	Alkyl
ILE299	5.27143	Hydrophobic	π-alkyl
PHE770	4.78202	Hydrophobic	π-alkyl

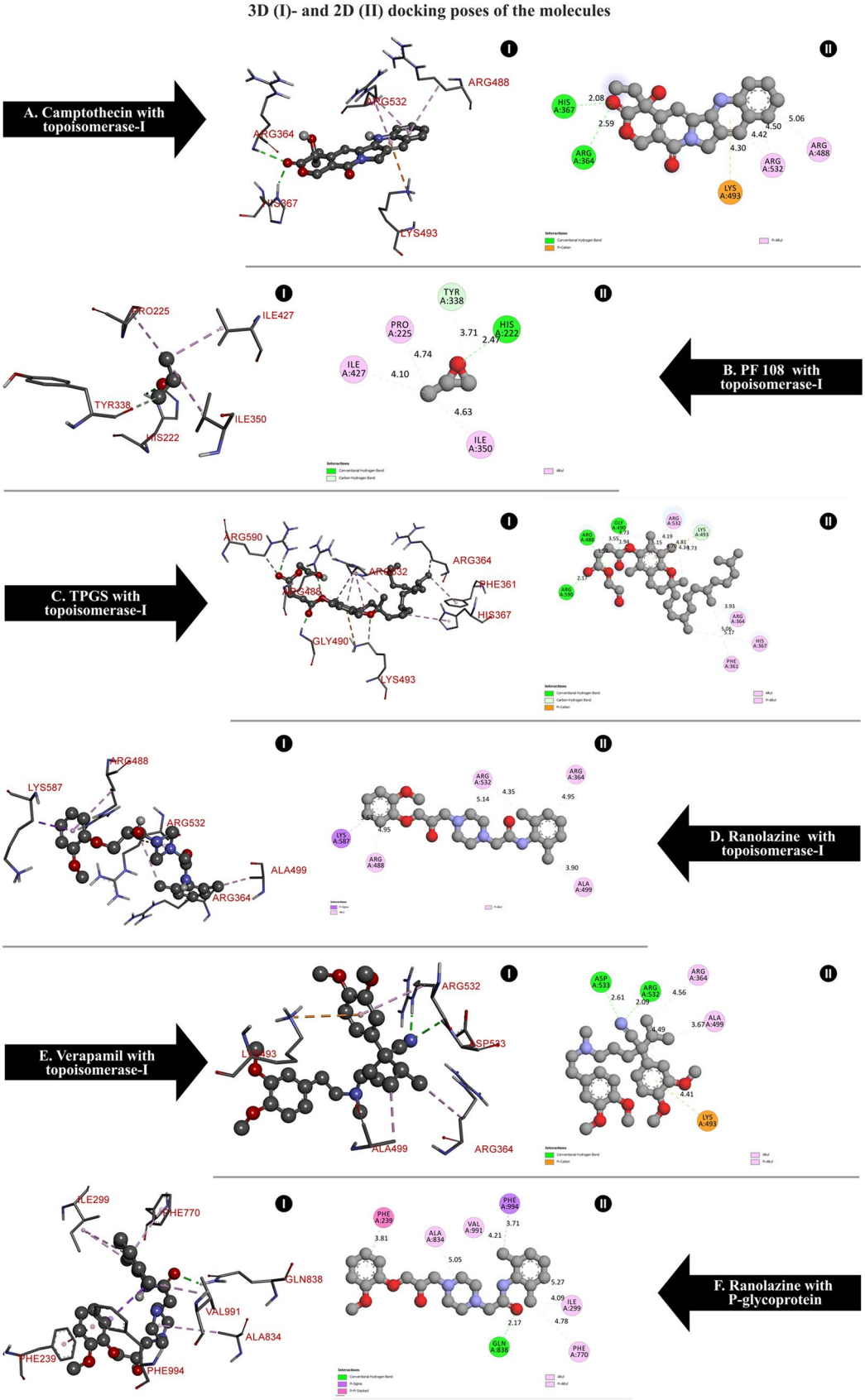

Fig. 5 The 3D and 2D docking poses of the molecules with topoisomares I and P-glycoprotein

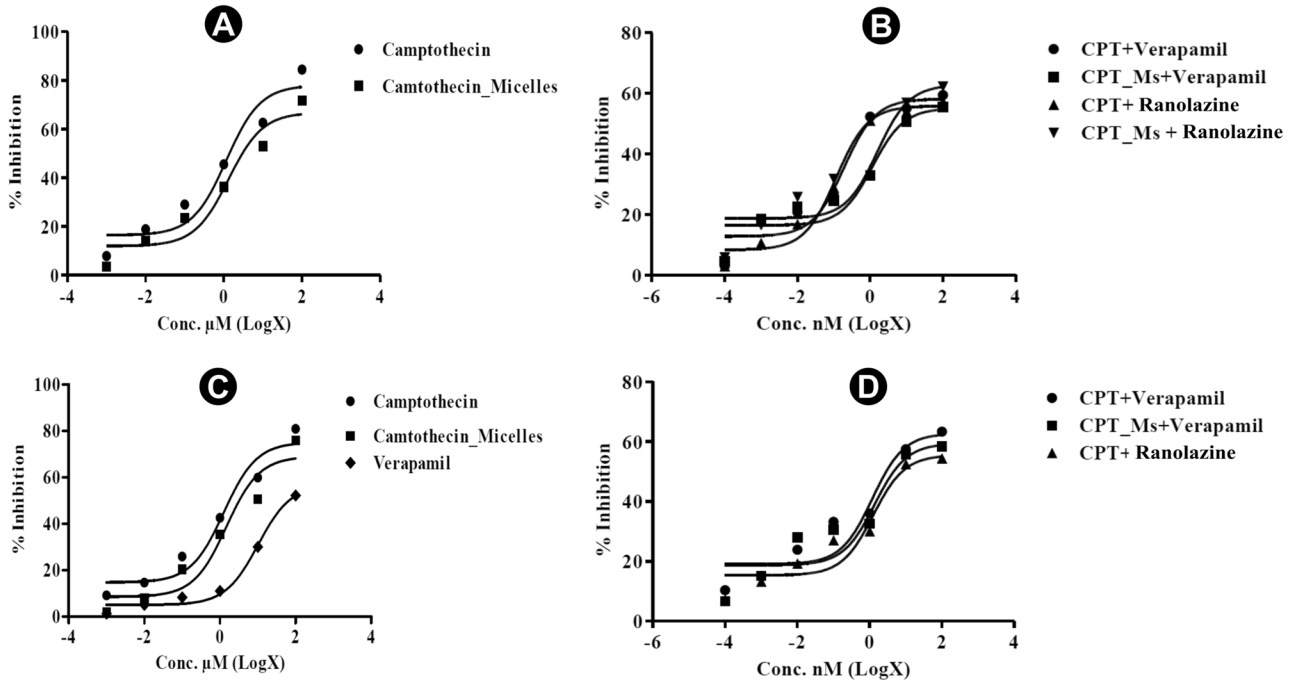

Fig. 6 % cell growth inhibition caused by various test samples. **(A)**, **(B)** Effect on mouse B16F10 melanoma cells and **(C)**, **(D)** effect on human A549 cells (CPT, camptothecin; CPT_Ms, camptothecin MMs)

chemotherapeutics such as camptothecin and its MMs. This study is a preliminary investigation wherein the non-micellar forms of verapamil and ranolazine are initially screened for their influence on the cytotoxicity of the micellar form of camptothecin. However, the study of the influence of micellar forms of these drugs could also be tested separately. As verapamil and ranolazine are safer drugs and do not cause toxicity to healthy cells as chemotherapeutics generally do, these can also be administered orally as conventional dosage forms that are available commercially. However, the use of verapamil and ranolazine in nanoparticulate form or conventional dosage forms is another topic of research. Thus, the present study is aimed to test their influence in non-micellar forms only.

Table 4 IC_{50} values of test samples against mouse B16F10 melanoma and human A549 cells after 48-h treatment

Samples	IC_{50} values	
	Cell lines	
	B16F10	A549
Plain camptothecin (µM)	1.168 ± 0.021	1.272 ± 0.051
Plain verapamil (µM)	Low inhibition	10.23
Plain ranolazine (µM)	Low inhibition	Low inhibition
Camptothecin MMs (µM)	1.329 ± 0.08	1.49 ± 0.043
Camptothecin (1 nM) in combination with varied moles (nM) of Verapamil	0.1925 ± 0.018***	1.191 ± 0.024
Camptothecin MMs (1 nM) in combination with varied moles (nM) of Verapamil	1.158 ± 0.0268	1.39 ± 0.018
Camptothecin (1 nM) in combination with varied moles (nM) of Ranolazine	0.1166 ± 0.068***	1.266 ± 0.015
Camptothecin MMs (1 nM) in combination with varied moles (nM) Ranolazine	1.592 ± 0.0812	Low inhibition

The values presented are mean ± SD ($n = 3$)

*** $p < 0.001$; p, significant when compared to campothecin MMs in combinations with varied moles of verapamil and ranolazine, respectively

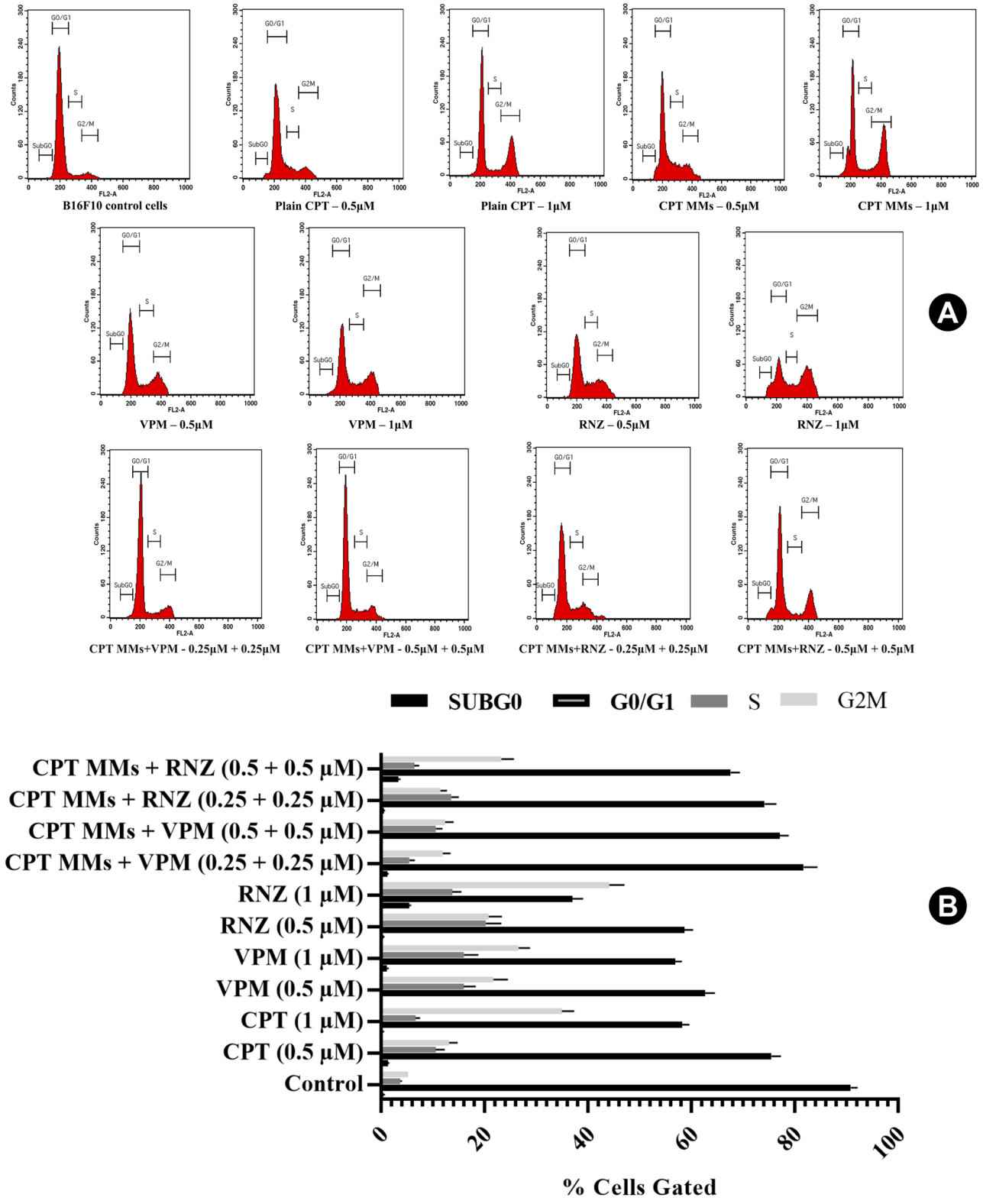

Fig. 7 **(A)** Flow cytometry histogram and **(B)** showing % B16F10 cells gated after 48-h of treatment with different samples

Cell Cycle Analysis

Cell cycle deregulation is one of the hallmarks of tumor cells. Thus, the induction of cell cycle arrest could be an effective approach to controlling the abnormal proliferation of tumor cells [86]. In the current study, the B16F10 cell cycle arresting behavior of camptothecin, verapamil, ranolazine, camptothecin MMs, camptothecin MMs + verapamil, and CPT MMs + ranolazine has been determined. The percentage of B16F10 cells arrested in Sub G0, G0/G1, S, and G2-M phase after 48 h treatment with the above test samples at different concentrations is presented in Fig. 7. The camptothecin caused substantially higher cell arrest in S and G2-M phase at 0.5 µM concentration when compared to control cells. At higher concentrations (1 µM), the 2.66-fold higher cell arrest is observed in G2-M phase when compared to 0.5 µM. The CPT MMs showed a similar pattern but even better cell arrest than camptothecin.

The verapamil and ranolazine caused moderately higher cell arrest at the S phase and significantly ($p < 0.05$) higher in G2-M phase at a lower concentration (0.5 µM) when compared to the anticancer drug camptothecin. The verapamil at 1 µM caused no significant changes in cell arrest at the S phase and G2-M phase when compared to 0.5 µM, whereas ranolazine caused 2.1-fold higher cell arrest in G2-M phase when compared to 0.5 µM. Ranolazine is found to show a similar pattern but even better cell arrest at 1 µM when compared to the standard anticancer drug camptothecin. These obtained results could be correlated to the ability of these drugs to induce microtubule damage, which results in prolonged G2-M arrest [87, 88]. The ability of ranolazine to arrest B16F10 cells at G2-M phase indicates its potential clinical application in the treatment of cancer.

In the present study, the cell cycle arresting behavior of camptothecin MMs in combination with verapamil and ranolazine is also screened to understand the combination effect. The combination effects are found lesser than the individual drugs. The camptothecin MMs plus ranolazine combination showed substantially higher cell arresting behavior than camptothecin MMs plus verapamil combination. Further molecular mechanism–based studies are needed to identify the exact reasons behind the decreased cell cycle arresting behaviors of these combinations. Besides, the cell cycle arresting behaviors of these combinations at higher concentrations need to be studied and validated using A549 and other cancer cell lines.

Conclusion

In the current research, the camptothecin-loaded MMs were developed and characterized in vitro for their suitability to treat cancer. The present study is a preliminary investigation that revealed the superior anticancer effect of camptothecin and its MMs at lower concentrations when combined with lower concentrations of verapamil and ranolazine. The in silico P-gp inhibitory actions of PF 108, TPGS, verapamil, and ranolazine indicated the potential application of the above combinations in the treatment of drug-resistant cancers. However, although the current study investigates the anticancer effect in non-resistant cells, further studies are required to validate the effectiveness of this combination in drug-resistant cancer cells. Furthermore, in silico topoisomerase-I inhibition activities of PF 108, TPGS, verapamil, and ranolazine need to be validated using cell culture and animal tumor models. Although the current study revealed the almost equal anticancer activities of the above combinations, further in vivo elaborative and mechanistic-based studies are required to evaluate the repurposing potential of verapamil or ranolazine with camptothecin or its MMs. The current study investigates the in vitro anticancer effect of test substances using non-resistant cells (B16F10 and A549). However, further studies are required to validate the effectiveness of the tested substances against camptothecin-resistant cancer cells.

Acknowledgements The authors are grateful to Bharati Vidyapeeth College of Pharmacy, Kolhapur, India, and Tatyasaheb Kore College of Pharmacy, Warananagar, for providing guidance and research facilities. Dr. Yogisha S. The Director, Skanda Life Sciences Pvt. Ltd., Bangalore, is to be thanked for providing the laboratory facilities for all cell culture studies.

Data Availability Not applicable.

Declarations

Conflict of Interest The authors declare no competing interests.

References

1. Cancer [Internet]. [cited 2021 Oct 6]. Available from: https://www.who.int/news-room/fact-sheets/detail/cancer
2. Prasher P, Sharma M, Dua K. Hyaluronic acid decorated naringenin nanoparticles: appraisal of chemopreventive and curative potential for lung cancer. Pharmaceutics. 2018;10. https://doi.org/10.3390/PHARMACEUTICS10010033.
3. Mandal B, Mittal N, Balabathula P, Thoma L, Wood G. Development and *in vitro* evaluation of core-shell type lipid-polymer hybrid nanoparticles for the delivery of erlotinib in non-small cell lung cancer. Eur J Pharm Sci. 2016;81:162–71. https://doi.org/10.1016/J.EJPS.2015.10.021.
4. Cheng W, Liang C, Xu L, Liu G, Gao N, Tao W, Luo L, et al. TPGS-functionalized polydopamine-modified mesoporous silica as drug nanocarriers for enhanced lung cancer chemotherapy against multidrug resistance. Small. 2017;13. https://doi.org/10.1002/SMLL.201700623.
5. Kusari S, Zühlke S, Spiteller M. An endophytic fungus from Camptotheca acuminata that produces camptothecin and

analogues. J Nat Prod. 2009;72:2–7. https://doi.org/10.1021/NP800455B.
6. Wall ME, Wani MC. Camptothecin and taxol: discovery to clinic—thirteenth Bruce F. Cain memorial award lecture. Cancer Res. 1995;55.
7. Giovanella BC, Hinz HR, Kozielski AJ, Stehlin JS, Silber R, Potmesil M. Complete growth inhibition of human cancer xenografts in nude mice by treatment with 20-(S)-camptothecin. Cancer Res. 1991;51.
8. Rivory LP, Robert J. Molecular, cellular, and clinical aspects of the pharmacology of 20(S)camptothecin and its derivatives. Pharmacol Ther Pergamon. 1995;68:269–96. https://doi.org/10.1016/0163-7258(95)02009-8.
9. Staker BL, Feese MD, Cushman M, Pommier Y, Zembower D, Stewart L, Burgin AB, et al. Structures of three classes of anticancer agents bound to the human topoisomerase I-DNA covalent complex. J Med Chem. 2005;48:2336–45. https://doi.org/10.1021/JM049146P.
10. Assali M, Cid J-J, Pernía-Leal M, Muñoz-Bravo M, Fernández I, Wellinger RE, et al. Glyconanosomes: disk-shaped nanomaterials for the water solubilization and delivery of hydrophobic molecules. ACS Nano Am Chem Soc. 2013;7:2145–53.
11. Kawano K, Watanabe M, Yamamoto T, Yokoyama M, Opanasopit P, Ok T, et al. Enhanced antitumor effect of camptothecin loaded in long-circulating polymeric micelles. J Control Release. 2006;112:329–32. https://doi.org/10.1016/J.JCONREL.2006.03.012.
12. Chiu Y-H, Hsu S-H, Hsu H-W, Huang K-C, Liu W, Wu C-Y, et al. Human non-small cell lung cancer cells can be sensitized to camptothecin by modulating autophagy. Int J Oncol Spandidos Publ. 2018;53:1967–79. https://doi.org/10.3892/IJO.2018.4523.
13. Nanayakkara AK, Follit CA, Chen G, Williams NS, Vogel PD, Wise JG. Targeted inhibitors of P-glycoprotein increase chemotherapeutic-induced mortality of multidrug resistant tumor cells. Sci Rep Nature Publishing Group. 2018;8:1–18. https://doi.org/10.1038/s41598-018-19325-x.
14. Zhang Y, Sriraman SK, Kenny HA, Luther E, Torchilin V, Lengyel E. Reversal of chemoresistance in ovarian cancer by co-delivery of a P-glycoprotein inhibitor and paclitaxel in a liposomal platform. Mol Cancer Ther. American Association for Cancer Research Inc.; 2016;15:2282–93. https://doi.org/10.1158/1535-7163.MCT-15-0986.
15. Dadwal A, Baldi A, Narang RK. Nanoparticles as carriers for drug delivery in cancer. Artif Cells Nanomed Biotechnol. 2018;46:295–305. https://doi.org/10.1080/21691401.2018.1457039.
16. Hu CMJ, Aryal S, Zhang L. Nanoparticle-assisted combination therapies for effective cancer treatment. Ther Deliv. 2010;1:323–34. https://doi.org/10.4155/TDE.10.13.
17. Palazzolo S, Bayda S, Hadla M, Caligiuri I, Corona G, Toffoli G, Rizzolio F, et al. The clinical translation of organic nanomaterials for cancer therapy: a focus on polymeric nanoparticles, micelles, liposomes and exosomes. Curr Med Chem. 2018;25:4224–68. https://doi.org/10.2174/0929867324666170830113755.
18. Xu C, Wang Y, Guo Z, Chen J, Lin L, Wu J, Tian H, Chen X, et al. Pulmonary delivery by exploiting doxorubicin and cisplatin co-loaded nanoparticles for metastatic lung cancer therapy. J Control Release. 2019;295:153–63. https://doi.org/10.1016/J.JCONREL.2018.12.013.
19. Soni V, Pandey V, Asati S, Gour V, Tekade RK. Biodegradable block copolymers and their applications for drug delivery. Basic Fundam Drug Deliv. Academic Press; 2019;401–47. https://doi.org/10.1016/B978-0-12-817909-3.00011-X.
20. Hare JI, Lammers T, Ashford MB, Puri S, Storm G, Barry ST. Challenges and strategies in anti-cancer nanomedicine development: an industry perspective. Adv Drug Deliv Rev Elsevier. 2017;108:25–38. https://doi.org/10.1016/J.ADDR.2016.04.025.
21. Manjappa AS, Kumbhar PS, Patil AB, Disouza JI, Patravale VB. Polymeric mixed micelles: improving the anticancer efficacy of single-copolymer micelles. Crit Rev Ther Drug Carrier Syst. Begell House Inc.; 2019;36:1–58. https://doi.org/10.1615/CritRevTherDrugCarrierSyst.2018020481.
22. Ebrahim Attia AB, Ong ZY, Hedrick JL, Lee PP, Ee PLR, Hammond PT, et al. Mixed micelles self-assembled from block copolymers for drug delivery. Curr Opin Colloid Interface Sci Elsevier. 2011;16:182–94. https://doi.org/10.1016/J.COCIS.2010.10.003.
23. Aw MS, Kurian M, Losic D. Polymeric micelles for multidrug delivery and combination therapy. Chem - A Eur J. John Wiley & Sons, Ltd; 2013;19:12586–601. https://doi.org/10.1002/chem.201302097.
24. Patil KS, Hajare AA, Manjappa AS, More HN, Disouza JI. Design, development, in silico and in vitro characterization of Docetaxel-loaded TPGS/ Pluronic F 108 mixed micelles for improved cancer treatment. J Drug Deliv Sci Technol. Elsevier; 2021;65:102685. https://doi.org/10.1016/J.JDDST.2021.102685.
25. Gao Y, Li LB, Zhai G. Preparation and characterization of Pluronic/TPGS mixed micelles for solubilization of camptothecin. Colloids Surf B Biointerfaces. 2008;64:194–9. https://doi.org/10.1016/J.COLSURFB.2008.01.021.
26. Onishi H, Machida Y, Machida Y. Antitumor properties of irinotecan-containing nanoparticles prepared using poly(DL-lactic acid) and poly(ethylene glycol)-block-poly(propylene glycol)-block-poly(ethylene glycol). Biol Pharm Bull. 2003;26:116–9. https://doi.org/10.1248/bpb.26.116.
27. Kunii R, Onishi H, Machida Y. Preparation and antitumor characteristics of PLA/(PEG-PPG-PEG) nanoparticles loaded with camptothecin. Eur J Pharm Biopharm. 2007;67:9–17. https://doi.org/10.1016/j.ejpb.2007.01.012.
28. Kunii R, Onishi H, Ueki KI, Koyama KI, Machida Y. Particle characteristics and biodistribution of camptothecin-loaded PLA/(PEG-PPG-PEG) nanoparticles. Drug Deliv Taylor & Francis. 2008;15:3–10. https://doi.org/10.1080/10717540701827154.
29. Sambamoorthy U, Manjappa AS, Eswara BRM, Sanapala AK, Nagadeepthi N. Vitamin E oil incorporated liposomal melphalan and simvastatin: approach to obtain improved physicochemical characteristics of hydrolysable melphalan and anticancer activity in combination with simvastatin against multiple myeloma. AAPS PharmSciTech 2021 231. Springer; 2021;23:1–16. https://doi.org/10.1208/S12249-021-02177-6.
30. Mahmoudi R, Hassandokht F, Ardakani MT, Karimi B, Roustazadeh A, Tarvirdipour S, et al. Intercalation of curcumin into liposomal chemotherapeutic agent augments apoptosis in breast cancer cells. J Biomater Appl. 2021;35:1005–18. https://doi.org/10.1177/0885328220976331.
31. Guimarães D, Noro J, Silva C, Cavaco-Paulo A, Nogueira E. Protective effect of saccharides on freeze-dried liposomes encapsulating drugs. Front Bioeng Biotechnol. Frontiers Media S.A.; 2019;7:424. https://doi.org/10.3389/FBIOE.2019.00424/FULL.
32. Kumbhar PS, Nadaf S, Manjappa AS, Jha NK, Shinde SS, Chopade SS, et al. D-α-tocopheryl polyethylene glycol succinate: a review of multifarious applications in nanomedicines. OpenNano. Elsevier Inc.; 2022;6. https://doi.org/10.1016/J.ONANO.2022.100036.
33. Pushpakom S, Iorio F, Eyers PA, Escott KJ, Hopper S, Wells A, et al. Drug repurposing: progress, challenges and recommendations. Nat Rev Drug Discov. 2019;18:41–58. https://doi.org/10.1038/NRD.2018.168.
34. Pantziarka P. Scientific advice - is drug repurposing missing a trick? Nat Rev Clin Oncol. 2017;14(455–6):455–6. https://doi.org/10.1038/NRCLINONC.2017.69.
35. Nosengo N. Can you teach old drugs new tricks? Nature. 2016;534:314–6. https://doi.org/10.1038/534314A.

36. Clohessy JG, Pandolfi PP. Mouse hospital and co-clinical trial project--from bench to bedside. Nat Rev Clin Oncol. 2015;12:491–8. https://doi.org/10.1038/NRCLINONC.2015.62.
37. Maxmen A. Busting the billion-dollar myth: how to slash the cost of drug development. Nature. 2016;536:388–90. https://doi.org/10.1038/536388A.
38. Bertolini F, Sukhatme VP, Bouche G. Drug repurposing in oncology–patient and health systems opportunities. Nat Rev Clin Oncol. 2015;12:732–42. https://doi.org/10.1038/NRCLINONC.2015.169.
39. Yang Y, Ma L, Xu Y, Liu Y, Li W, Cai J, et al. Enalapril overcomes chemoresistance and potentiates antitumor efficacy of 5-FU in colorectal cancer by suppressing proliferation, angiogenesis, and NF-κB/STAT3-regulated proteins. Cell Death Dis Springer Nature. 2020;11:1–13. https://doi.org/10.1038/s41419-020-2675-x.
40. Wong BS, Chiu LY, Tu DG, Sheu GT, Chan TT. Anticancer effects of antihypertensive l-type calcium channel blockers on chemoresistant lung cancer cells via autophagy and apoptosis. Cancer Manag Res. Dove Medical Press Ltd; 2020;12:1913–27. https://doi.org/10.2147/CMAR.S228718.
41. De Souza VB, Silva EN, Ribeiro ML, De Martins WA. Hypertension in patients with cancer. Arq Bras Cardiol 2015;246–52. https://doi.org/10.5935/abc.20150011.
42. Wegman-Ostrosky T, Soto-Reyes E, Vidal-Millán S, Sánchez-Corona J. The renin-angiotensin system meets the hallmarks of cancer. JRAAS - J. Renin-Angiotensin-Aldosterone Syst. SAGE Publications Ltd; 2015. p. 227–33. https://doi.org/10.1177/1470320313496858.
43. George AJ, Allen A, Chand AL. Repurposing ARBs as treatments for breast cancer. Aging (Albany NY). 2017;9:1357–8. https://doi.org/10.18632/AGING.101249.
44. Carlos-Escalante JA, de Jesús-Sánchez M, Rivas-Castro A, Pichardo-Rojas PS, Arce C, Wegman-Ostrosky T. The use of antihypertensive drugs as coadjuvant therapy in cancer. Front Oncol Front Media SA. 2021;11:1595. https://doi.org/10.3389/FONC.2021.660943/BIBTEX.
45. Bellamy WT. Annu Rev pharmacol toxicol. 1996;36:161–83. https://doi.org/10.1146/annurev.pa.36.040196.001113.
46. Broxterman HJ, Lankelma J, Pinedo HM. How to probe clinical tumour samples for P-glycoprotein and multidrug resistance-associated protein. Eur J Cancer. 1996;32A:1024–33. https://doi.org/10.1016/0959-8049(96)00045-7.
47. Ince P, Appleton DR, Finney KJ, Sunter JP, Watson AJ. Verapamil increases the sensitivity of primary human colorectal carcinoma tissue to vincristine. Br J Cancer. Nature Publishing Group; 1986;53:137. https://doi.org/10.1038/BJC.1986.19.
48. Merry S, Fetherston CA, Kaye SB, Freshney RI, Plumb JA. Resistance of human glioma to adriamycin in vitro: the role of membrane transport and its circumvention with verapamil. Br J Cancer. Nature Publishing Group; 1986;53:129. https://doi.org/10.1038/BJC.1986.18.
49. Belpomme D, Gauthier S, Pujade-Lauraine E, Facchini T, Goudier MJ, Krakowski I, et al. Verapamil increases the survival of patients with anthracycline-resistant metastatic breast carcinoma. Ann Oncol Elsevier. 2000;11:1471–6. https://doi.org/10.1023/A:1026556119020.
50. Tsuruo T, Iida H, Tsukagoshi S SY. Overcoming of vincristine resistance in P388 leukemia in vivo and in vitro through enhanced cytotoxicity of vincristine and vinblastine by verapamil. Cancer Res. 1981;May;41:1967–72.
51. Zhao L, Zhao Y, Schwarz B, Mysliwietz J, Hartig R, Camaj P, et al. Verapamil inhibits tumor progression of chemotherapyresistant pancreatic cancer side population cells. Int J Oncol Spandidos Publications. 2016;49:99–110. https://doi.org/10.3892/ijo.2016.3512.
52. Bugan I, Kucuk S, Karagoz Z, Fraser SP, Kaya H, Dodson A, et al. Anti-metastatic effect of ranolazine in an in vivo rat model of prostate cancer, and expression of voltage-gated sodium channel protein in human prostate. Prostate Cancer Prostatic Dis. Nature Publishing Group; 2019;22:569–79. https://doi.org/10.1038/S41391-019-0128-3.
53. Rouhana S, Virsolvy A, Fares N, Richard S, Thireau J. Ranolazine: an old drug with emerging potential; lessons from pre-clinical and clinical investigations for possible repositioning. Pharm 2022, Vol 15, Page 31. Multidisciplinary Digital Publishing Institute; 2021;15:31. https://doi.org/10.3390/PH15010031.
54. Tocchetti CG, Carpi A, Coppola C, Quintavalle C, Rea D, Campesan M, et al. Ranolazine protects from doxorubicin-induced oxidative stress and cardiac dysfunction. Eur J Heart Fail. 2014;16:358–66. https://doi.org/10.1002/EJHF.50.
55. Cappetta D, Esposito G, Coppini R, Piegari E, Russo R, Ciuffreda LP, et al. Effects of ranolazine in a model of doxorubicin-induced left ventricle diastolic dysfunction. Br J Pharmacol. 2017;174:3696–712. https://doi.org/10.1111/BPH.13791.
56. Riccio G, Antonucci S, Coppola C, D'Avino C, Piscopo G, Fiore D, et al. Ranolazine attenuates trastuzumab-induced heart dysfunction by modulating ROS production. Front Physiol. 2018;9. https://doi.org/10.3389/FPHYS.2018.00038.
57. Minotti G, Menna P, Calabrese V, Greco C, Armento G, Annibali O, et al. Pharmacology of ranolazine versus common cardiovascular drugs in patients with early diastolic dysfunction induced by anthracyclines or nonanthracycline chemotherapeutics: a phase 2b minitrial. J Pharmacol Exp Ther Am Soc Pharmacol Exp Ther. 2019;370:197–205. https://doi.org/10.1124/JPET.119.258178.
58. Gonzalez RJ, Tarloff JB. Evaluation of hepatic subcellular fractions for alamar blue and MTT reductase activity. Toxicol In Vitro. 2001;15:257–9. https://doi.org/10.1016/S0887-2333(01)00014-5.
59. Han Z, Qian-Qian F, Jian-Hua G, Jing-Ping MJPM. Anticancer effects of isofraxidin against A549 human lung cancer cells via the EGFR signaling pathway. Mol Med Rep. 2018;18:407–14. https://doi.org/10.3892/MMR.2018.8950.
60. Dallakyan S, Olson AJ. Small-molecule library screening by docking with PyRx. Methods Mol Biol. 2015;1263:243–50. https://doi.org/10.1007/978-1-4939-2269-7_19.
61. Rappé AK, Casewit CJ, Colwell KS, Goddard WA, Skiff WM. UFF, a full periodic table force field for molecular mechanics and molecular dynamics simulations. J Am Chem Soc. 1992;114:10024–35. https://doi.org/10.1021/ja00051a040.
62. Gaisford S, Beezer AE, Mitchell JC, Loh W, Finnie JK, Williams SJ. Diode-array UV spectrometric evidence for a concentration dependent phase transition in dilute aqueous solutions of pluronic F87 (poloxamer 237). J Chem Soc Chem Commun. 1995;1843–4. https://doi.org/10.1039/C39950001843.
63. Wei Z, Hao J, Yuan S, Li Y, Juan W, Sha X, et al. Paclitaxel-loaded pluronic P123/F127 mixed polymeric micelles: formulation, optimization and in vitro characterization. Int J Pharm Int J Pharm. 2009;376:176–85. https://doi.org/10.1016/j.ijpharm.2009.04.030.
64. Manjappa AS, Kumbhar PS, Khopade PS, Patil AB, Disouza JI. Mixed micelles as nano polymer therapeutics of docetaxel: increased in vitro cytotoxicity and decreased in vivo toxicity. Curr Drug Deliv. 2018;15:564–75. https://doi.org/10.2174/1567201814666170621113637.
65. Jörgen J, Karin S, Gerd O, da Silva RC, Watson L. The Interaction between PEO-PPO-PEO triblock copolymers and ionic surfactants in aqueous solution studied using light scattering and calorimetry. J Phys Chem B Am Chem Soc. 2003;108:82–92. https://doi.org/10.1021/JP030792U.
66. Morteza-Semnani K, Saeedi M, Akbari J, Eghbali M, Babaei A, Hashemi SMH, et al. Development of a novel nanoemulgel formulation containing cumin essential oil as skin permeation

enhancer. Drug Deliv Transl Res 2021. Springer; 2021;1–11. https://doi.org/10.1007/S13346-021-01025-1.
67. Koo OM, Rubinstein I, Onyuksel H. Camptothecin in sterically stabilized phospholipid micelles: a novel nanomedicine. Nanomedicine Nanotechnology, Biol Med. 2005;1:77–84. https://doi.org/10.1016/J.NANO.2004.11.002.
68. Hajare AA, More HN, Pisal SS. Effect of sugar additives on stability of human serum albumin during vacuum foam drying and storage. Curr Drug Deliv. Bentham Science Publishers Ltd.; 2011;8:678–90. https://doi.org/10.2174/156720111797635450.
69. Jindal N, Mehta SK. Nevirapine loaded Poloxamer 407/Pluronic P123 mixed micelles: optimization of formulation and in vitro evaluation. Colloids Surf B Biointerfaces. Elsevier B.V.; 2015;129:100–6. https://doi.org/10.1016/j.colsurfb.2015.03.030.
70. Christiana MN, Constantina C, Panagiotis P, Andreas IC. D-alpha-tocopheryl polyethylene glycol succinate (TPGS) induces cell cycle arrest and apoptosis selectively in Survivin-overexpressing breast cancer cells. Biochem Pharmacol. 2014;89:31–42. https://doi.org/10.1016/J.BCP.2014.02.003.
71. Shi L, Song XB, Wang Y, Wang KT, Liu P, Pang B, et al. Docetaxel-conjugated monomethoxy-poly(ethylene glycol)-: B -poly(lactide) (mPEG-PLA) polymeric micelles to enhance the therapeutic efficacy in oral squamous cell carcinoma. RSC Adv Royal Soc Chem. 2016;6:42819–26. https://doi.org/10.1039/c6ra03332f.
72. Khan SL, Siddiqui FA, Jain SP, Sonwane GM. Discovery of potential inhibitors of SARS-CoV-2 (COVID-19) main protease (Mpro) from Nigella Sativa (Black Seed) by molecular docking study. Coronaviruses. Bentham Science Publishers Ltd.; 2020;01. https://doi.org/10.2174/2666796701999200921094103.
73. Kumbhar PS, Birange S, Atavale M, Disouza JI, Manjappa AS. d-Gluconic acid–based methotrexate prodrug–loaded mixed micelles composed of MDR reversing copolymer: in vitro and in vivo results. Colloid Polym Sci Springer Verlag. 2018;296:1971–81. https://doi.org/10.1007/s00396-018-4416-6.
74. Manjappa AS, Kumbhar PS, Kasabe R, Diwate SK, Disouza JI. Ameliorated in vitro anticancer efficacy of methotrexate d-α-tocopheryl polyethylene glycol 1000 succinate ester against breast cancer cells. Futur J Pharm Sci 2019 51. SpringerOpen; 2019;5:1–10. https://doi.org/10.1186/S43094-019-0013-X.
75. Bandgar SA, Jadhav NR, Manjappa AS. A remarkable in vitro cytotoxic, cell cycle arresting and proapoptotic characteristics of low-dose mixed micellar simvastatin combined with alendronate sodium. Drug Deliv Transl Res Springer. 2020;10:1122–35. https://doi.org/10.1007/s13346-020-00752-1.
76. Zhang Z, Tan S, Feng SS. Vitamin E TPGS as a molecular biomaterial for drug delivery. Biomaterials. 2012. p. 4889–906. https://doi.org/10.1016/j.biomaterials.2012.03.046.
77. Mu L, Elbayoumi TA, Torchilin VP. Mixed micelles made of poly(ethylene glycol)-phosphatidylethanolamine conjugate and d-alpha-tocopheryl polyethylene glycol 1000 succinate as pharmaceutical nanocarriers for camptothecin. Int J Pharm. 2005;306:142–9. https://doi.org/10.1016/J.IJPHARM.2005.08.026.
78. Chandran T, Katragadda U, Teng Q, Tan C. Design and evaluation of micellar nanocarriers for 17-allyamino-17-demethoxygeldanamycin (17-AAG). Int J Pharm. 2010;392:170–7. https://doi.org/10.1016/J.IJPHARM.2010.03.056.
79. Bhuptani RS, Jain AS, Makhija DT, Jagtap AG, Rahiman Hassan PA, Nagarsenker MS. Soluplus based polymeric micelles and mixed micelles of lornoxicam: design, characterization and In vivo efficacy studies in rats. Indian J Pharm Educ Res. 2016;50:277–86.
80. Bandgar SA, Jadhav NR, Manjappa AS. A remarkable in vitro cytotoxic, cell cycle arresting and proapoptotic characteristics of low-dose mixed micellar simvastatin combined with alendronate sodium. Drug Deliv Transl Res. 2020;10:1122–35. https://doi.org/10.1007/S13346-020-00752-1.
81. Galatage ST, Hebalkar AS, Gote RV, Mali OR, Killedar SG, Bhagwat DA, et al. Design and characterization of camptothecin gel for treatment of epidermoid carcinoma. Futur J Pharm Sci 2020 61. SpringerOpen; 2020;6:1–11. https://doi.org/10.1186/S43094-020-00066-6.
82. Zhang L, Tan L, Chen L, Chen X, Long C, Peng J, et al. A simple method to improve the stability of docetaxel micelles. Sci Reports 2016 61. Nature Publishing Group. 2016;6:1–10. https://doi.org/10.1038/srep36957.
83. Dabholkar RD, Sawant RM, Mongayt DA, Devarajan PV, Torchilin VP. Polyethylene glycol-phosphatidylethanolamine conjugate (PEG-PE)-based mixed micelles: some properties, loading with paclitaxel, and modulation of P-glycoprotein-mediated efflux. Int J Pharm Int J Pharm. 2006;315:148–57. https://doi.org/10.1016/J.IJPHARM.2006.02.018.
84. Din FU, Aman W, Ullah I, Qureshi OS, Mustapha O, Shafique S, et al. Effective use of nanocarriers as drug delivery systems for the treatment of selected tumors. Int J Nanomed Dove Med Press Ltd. 2017;7291–309. https://doi.org/10.2147/IJN.S146315.
85. Unnam S, Manjappa AS, Muddana Eswara BR, Salawi A, Gunti P. Liposomal melphalan: approach to obtain improved plasma stability, pharmacokinetics, and in vitro and in vivo anticancer efficacy in combination with liposomal simvastatin against mouse RPMI-8226 multiple myeloma model. J Drug Deliv Sci Technol Elsevier. 2022;73:103479. https://doi.org/10.1016/J.JDDST.2022.103479.
86. Zhao X, Qi T, Kong C, Hao M, Wang Y, Li J, et al. Photothermal exposure of polydopamine-coated branched Au–Ag nanoparticles induces cell cycle arrest, apoptosis, and autophagy in human bladder cancer cells. Int J Nanomed Dove Press. 2018;13:6413–28. https://doi.org/10.2147/IJN.S174349.
87. Wang T, Zhu D, Liu G, Tao W, Cao W, Zhang L, et al. DTX-loaded star-shaped TAPP-PLA-b-TPGS nanoparticles for cancer chemical and photodynamic combination therapy. RSC Adv Royal Soc Chem. 2015;5:50617–27. https://doi.org/10.1039/C5RA09042C.
88. Luo Y, Ling Y, Guo W, Pang J, Liu W, Fang Y, et al. Docetaxel loaded oleic acid-coated hydroxyapatite nanoparticles enhance the docetaxel-induced apoptosis through activation of caspase-2 in androgen independent prostate cancer cells. J Control Release. 2010;147:278–88. https://doi.org/10.1016/J.JCONREL.2010.07.108.